Macromolecules
NOTE

Macromolecules **2010**, *43*, 1665–1670 **1665**
DOI: 10.1021/ma9020196

Bending of Lamellar Microdomains of Block Copolymers on Nonselective Surfaces

Sang-Min Park,[†] Meng Dong,[‡] Charles T. Rettner,[†] David S. Dandy,[‡] Qiang Wang,*[,‡] and Ho-Cheol Kim*[,†]

[†]*IBM Research Division, Almaden Research Center, 650 Harry Road, San Jose, California 95120 and* [‡]*Department of Chemical and Biological Engineering, Colorado State University, 1370 Campus Delivery, Fort Collins, Colorado 80523*

Received September 9, 2009; Revised Manuscript Received November 19, 2009

Introduction

Symmetric diblock copolymers self-assemble into lamellar microdomains which can be used to create line and space patterns on substrates by controlling the orientation of microdomains.[1−4] Previously, it has been reported that the orientation of lamellar microdomains can be controlled perpendicular to the surface by modifying the substrate surface to become nonselective to each domain.[5,6] For practical use of the block copolymer based patterns for nanofabrications, of great interest is precise control over the lateral placement of lamellar microdomains. Commonly predefined guiding patterns containing chemical and/or topographical contrast have been used to direct the lateral placement of lamellae on substrates.[7−18]

In the absence of guiding patterns, the lamella microdomains produce fingerprint-like surface patterns on nonselective substrates as reported previously with a variety of model diblock copolymers, where the most well-studied diblock copolymer is poly(styrene-*b*-methyl methacrylate) (PS-*b*-PMMA).[7−9,11,13,14,16−18] The fact that this fingerprint-like pattern contains many regions of high curvature of bent lamellae suggests the cost of lamellae bending may be relatively small.[14] Previously, Nealey and co-workers reported that the lamellar microdomains of PS-*b*-PMMA faithfully follow the lithographically predefined surface patterns of chemical contrast.[7,13] They showed that bent block copolymer lamellae could be obtained when homopolymers were added to the copolymer. More recently, Wilmes et al. examined the extent to which patterns with different curvatures can be created within the same block copolymer thin films.[14] They showed that the lamellae conform to patterns with radii of curvature equal to the equilibrium domain spacing. In this Note, we report our investigation on the bending characteristics of lamellar microdomains resulting from directed assembly using topographic guiding patterns. We designed the topographic guiding patterns as elbows with varying corner angles. By controlling the surface of guiding patterns nonselective to the microdomains, we rendered the orientation of lamellae perpendicular to the surfaces of bottom and sidewalls of the guiding patterns. Detailed experimental observation of the degree of bending and tilting of lamellae at the sidewall surface is reported along with a theoretical investigation using self-consistent-field calculations, which provide additional knowledge regarding the free energy and interfacial characteristics of the experimentally observed morphologies. We also extended our investigation to a block copolymer hybrid system which is a mixture of an organic diblock copolymer, poly(styrene-*b*-ethylene oxide) (PS-*b*-PEO), and an organosilicate (OS) resin.[19,20] The effect of larger orientational correlation length of the hybrid system on the bending property of lamellar microdomains will be discussed.

*To whom correspondence should be addressed. E-mail: hckim@us.ibm.com (H.-C.K), q.wang@colostate.edu (Q.W.).

Experimental Section

Materials. Symmetric poly(styrene-*b*-methyl methacrylate) (PS-*b*-PMMA) and asymmetric poly(styrene-*b*-ethylene oxide) (PS-*b*-PEO) were purchased from Polymer Source, Inc., and used as received. The number-averaged molecular weights (M_n) of PS-*b*-PMMA and PS-*b*-PEO were 36 kg/mol (18 kg/mol for PS, 18 kg/mol for PMMA) and 31.3 kg/mol (19 kg/mol for PS, 12.3 kg/mol for PEO), respectively. The organosilicate (OS) used in this work was a copolymer of methyltrimethoxysilane and tetraethylorthosilicate having molecular weight of about 2 kg/mol and T/Q ratio of 75/25. Nitroxide-mediated living free-radical polymerization was performed to synthesize a hydroxyl-terminated random copolymer of styrene and methyl methacrylate (PS-*r*-PMMA) with 58 vol % styrene. Polymethylglutarimide (PMGI SF2) was purchased from Microchem and used to prepare nonselective surface to PS-*b*-PEO/OS hybrid.

Fabrication of Substrates. The fabrication of topographic guiding patterns began with patterning a photoresist film of poly(methyl methacrylate) (PMMA, M_n = 950 kg/mol, Microchem) using electron beam lithography (Vistec VB6, 100 keV). After developing the photoresist patterns and rinsing with DI water, a 15 nm layer of chromium (Cr) was deposited by evaporation. Ultrasonication of the samples in *N*-methylpyrrolidone (NMP) for 15 min mechanically removed the remaining resist and the overlying deposited metal. This standard liftoff process resulted in 180 nm wide Cr features that were used as an etch mask for fabrication of channel-like patterns with varying dimensions. A reactive ion etch (RIE) with CF_4 gas was performed to etch unprotected regions of the SiO_2 substrate. After a 50 nm etch, the remaining Cr was removed using a commercial Cr etchant (Transene). The resulting structures were 50 nm high and formed elbow-like patterns that ranged in angle (θ) from 30° to 170° in 20° increments and in spacing from 200 to 800 nm.

Block Copolymer Thin Films. Details on the preparation of surface patterns using lamellar microdomains of PS-*b*-PEO/OS hybrid system have been described previously.[20] Here we briefly discuss the process. A 20 nm thick PMGI layer was deposited on the prepatterned substrates which are cleaned by UV/O_3 treatment. The PMGI layer serves as a nonselective surface to two domains of the hybrid, i.e., PS and PEO + OS. Propylene glycol monomethyl ether acetate (PGMEA) was used to prepare

Published on Web 01/08/2010

1 wt % solutions of PS-*b*-PEO and heated at 100 °C to dissolve the block copolymer completely. Then, PS-*b*-PEO solutions in PGMEA were mixed with 1 wt % OS solutions in propylene glycol propyl ether (PGPE) to prepare the hybrid solution. To generate the lamellar morphology of hybrid copolymers, the weight ratio of PS-*b*-PEO/OS was set to 55/45. After deposition of the hybrid copolymer solution onto the substrates, the system was held for 30 s under a toluene atmosphere and then spun at 2000 rpm for 45 s. The as-cast samples were subsequently baked at 180 °C for 30 min to cross-link OS as well as remove residual solvents.

For surface patterning of PS-*b*-PMMA, a thin layer of hydroxyl-terminated PS-*r*-PMMA was deposited onto UV/O_3 treated topographic patterns from 1 wt % PGMEA solution and then heated under nitrogen at 200 °C for 2 h. Unanchored PS-*r*-PMMA was rinsed away using PGMEA. A PGMEA solution of PS-*b*-PMMA was spun-cast to generate thin films on the substrate. Thickness of the PS-*b*-PMMA film was measured to be ~30 nm on the flat region of the substrate. The samples were subsequently placed on a hot plate and annealed at 190 °C for 24 h in a nitrogen environment. A previous study suggests that the PS-*b*-PMMA thin films show morphology close to equilibrium state under this annealing condition.[18]

Characterization. The resulting morphologies were imaged using a field emission scanning electron microscope (FESEM, LEO 1550 VP) under the acceleration voltage of 15 kV without any metal deposition. The evaluation of film thickness was performed with NanoSpec/AFT 4150 (Nanometrics Inc.).

Self-Consistent-Field Calculations. Since the polymer self-consistent-field (SCF) theory has been well developed, we only provide a brief summary of the SCF calculations here; readers are referred to, e.g., ref 21 for detailed derivation and explanation of this theory. To compare against the laboratory measurements, we perform two-dimensional SCF calculations in real space, without *a priori* knowledge of the possible morphologies. The formalism explicitly accounts for the conformational entropy of A-B diblock copolymer chains (modeled by Gaussian chains in external fields) and the repulsion between A and B segments (modeled by the Flory-Huggins χ parameter). In accordance with experiment conditions, the SCF calculations are performed at $\chi N = 25$, where $N = 733$ is the total number of segments on each PS-*b*-PMMA chain, and we assume the same statistical segment length of $a = 0.66$ nm and bulk density for both PS and PMMA segments.

Results and Discussion

Figure 1a schematically represents the experimental process for preparing samples. The process is simple and straightforward: (1) preparation of substrates with guiding elbow patterns; (2) deposition of nonselective layer on topographic guiding patterns of silicon followed by assembly of block copolymer (or block copolymer hybrid). Figure 1b shows detailed dimensions of the elbow-like topographic guiding patterns prepared by E-beam lithography. Elbow corner angle (θ) and gap between sidewalls are controlled from 30° to 170° and from 200 to 800 nm, respectively. The height of topographic guiding patterns was maintained at 50 nm and the length of linear section of the elbow patterns was 2 μm, which is far longer than the distance that a defect can propagate.[18]

PS-*b*-PEO/OS Hybrid on the Elbow Patterns. The characteristics of PS-*b*-PEO/OS hybrid material have been reported previously.[19,20] The material shows strong segregation between two microdomains due to the inorganic nature of the OS; hence, it extends the accessible dimensions of microdomains down to the sub-10 nm range. The high content of silicon in OS gives significantly improved plasma etching contrast, which makes process schemes for device fabrication much simpler. Compared to typical organic

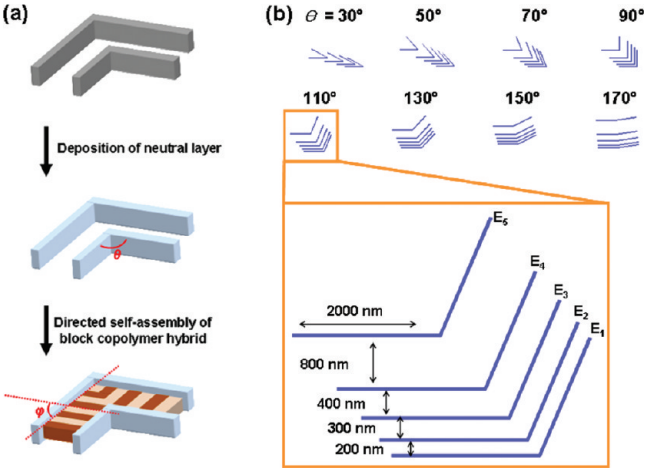

Figure 1. Schematic of the process used to direct the assembly of lamellae-forming block copolymers on topographic guiding patterns with bending geometries. (a) The procedure begins with the deposition of neutral layer followed by directed self-assembly of block copolymer thin films. (b) Diagram of topographic guiding patterns.

diblock copolymers such as PS-*b*-PMMA, the hybrid exhibits a lower number density of defects, partly due to the ~5 times larger orientational correlation length. Morphology and dimensions of microdomains can be readily tuned through the mixing composition and molecular weight of PS-*b*-PEO, respectively. The material composition used in this study yields lamellar microdomains of period $L_0 \approx 43$ nm. Figure 2a shows a series of plan-view SEM images of the hybrid lamellae guided by elbow patterns with different corner angles (θ). To evaluate the effect of individual elbow patterns on the ordering of lamellae, these images are taken from the most outer elbow patterns (E_5 in Figure 1b). The thick, brightest lines in the SEM images correspond to the E-beam guiding patterns, while thin gray and dark lines correspond to the PEO + OS and PS domains, respectively. It is noted that the lamellae align between two sidewalls of the elbows in such a way as to form arclike patterns. This behavior is observed with elbow patterns of the corner angle (θ) ranging from 30° to 110°. A transition in the alignment of lamellae takes place for $110° \leq \theta \leq 130°$. For elbow patterns with $\theta \geq 130°$, lamellar microdomains do not bend to connect the two sidewalls of the elbow pattern.

Figure 2b shows the bending behavior of lamellae in paired elbows, where the patterns are parallel with fixed gap distances (E_1 to E_4 in Figure 1b). We focused on the behavior of lamellar microdomains in 200 and 300 nm gaps as the lamellae in the patterns with the 400 nm gap show similar behavior to the individual elbow patterns described above. For both 200 and 300 nm gaps, we observed the lamellae align to the direction perpendicular to the sidewalls of the elbow patterns. Bent lamellae were observed near the corners of the elbow patterns. Note that the bending behavior of lamellae is different from the single elbow patterns in Figure 2a mainly due to the interaction between two parallel sidewalls of the paired elbow patterns. Bending of lamellae at the corner of the elbow patterns is observed for θ up to 130°. Defective patterns are observed at the corner when $\theta = 150°$. No significant effect of the elbow corner is observed with elbow patterns when $\theta = 170°$.

The large orientational correlation length of the PS-*b*-PEO/OS hybrid system makes it straightforward to observe the bending behavior of lamellae over relatively large areas.

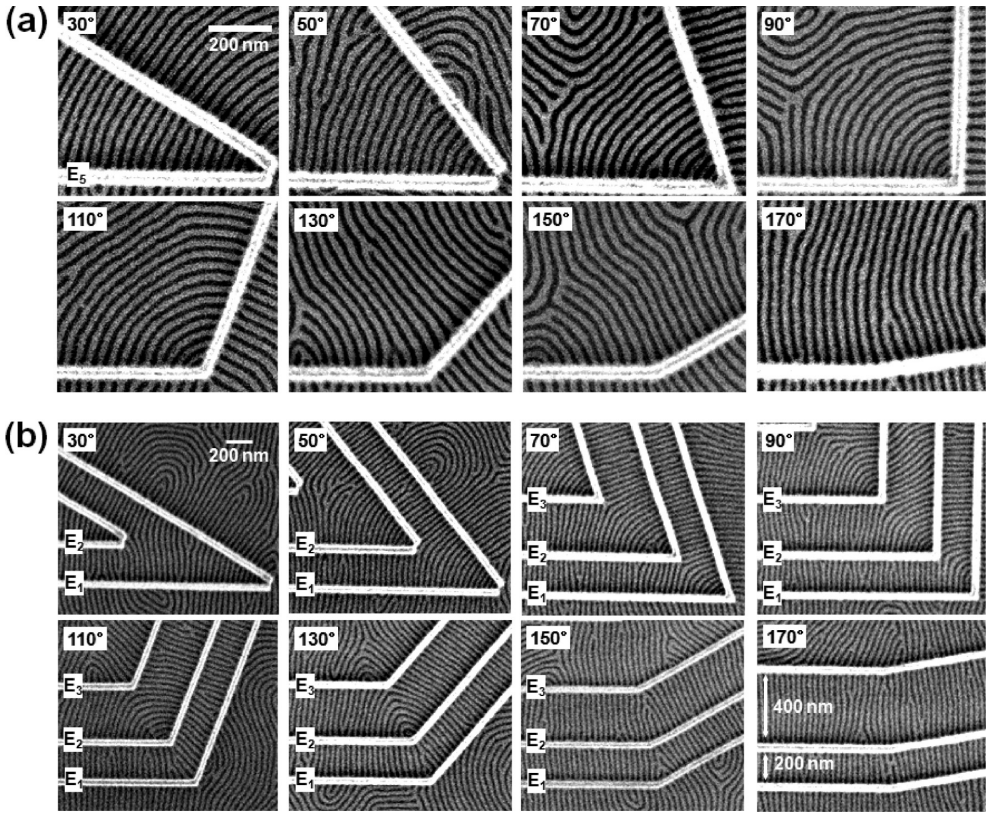

Figure 2. Top-down SEM images of lamellar microdomains in PS-*b*-PEO/OS thin films on (a) single and (b) paired elbow patterns with varying angles (θ) from 30° to 170° in 20° increments.

However, the morphology of this hybrid is not in equilibrium but rather kinetically trapped during spin-coating due to the strong repulsive interaction between the two microdomains. To investigate more detailed characteristics of lamellae bending under equilibrium (or near-equilibrium) conditions, we examined the behavior of a model organic diblock copolymer, poly(styrene-*b*-methyl methacrylate) (PS-*b*-PMMA).

PS-*b*-PMMA on the Elbow Patterns. Figure 3a shows plan-view SEM images of PS-*b*-PMMA on E_5 elbow patterns. For the molecular weight of PS-*b*-PMMA chosen for this study, we measured the lamellar period to be $L_0 = 28$ nm by 2D fast Fourier transformation (FFT). For the lamellar microdomains in Figure 3a, the bright and dark regions correspond to PS and PMMA microdomains, respectively. The number of lamellar microdomains bent at the corner is much less than in the hybrid system, e.g., 3 for PS-*b*-PMMA and 13 for PS-*b*-PEO/OS at 90°, even though PS-*b*-PMMA has smaller periodicity of lamellae, which is very likely due to the smaller orientational correlation length of PS-*b*-PMMA. It is interesting to note that the bending-unbending transition takes place over the same range of θ as the hybrid material, that is, 110° to 130°.

As shown in Figure 3b, we investigated the behavior of lamellar microdomains in paired (parallel) elbow patterns. Attention is focused on the 200 nm gap dimension because of the high number density of defects in lamellae observed in the gaps bigger than 300 nm. Similar to the behavior of the PS-*b*-PEO/OS hybrid, the linear portion of the parallel elbow patterns (gap between E_1 and E_2) is filled with lamellae aligned orthogonal to the sidewalls of the elbows. It is interesting to note that the angles between lamellae and the sidewalls are not exactly 90°, and they vary with the distance from the corner of elbow patterns. The plot in Figure 4 shows the average tilting angles (φ) of lamellae as a function of elbow corner angles θ. The tilting angle φ was measured for the fifth through seventh lamellae from the corner of the E_1 elbow patterns. As shown in Figure 4, φ values are not constant but exhibit maxima and minima within the range of θ investigated in this study. This behavior is likely due to the fact that the tilting angles are determined by the free energy, which is balanced with the degree of bending of lamellae induced by the elbow patterns with various corner angles. For a given value of θ, φ increases with the number of lamellar microdomains from the corner of elbow patterns. A simple geometric argument shows that $(\pi - \theta)/2$ give the lower limit of φ, and we note that our measured φ value at $\theta = 30°$ is subject to large error due to the presence of defects. More insights will be discussed below in connection with the self-consistent-field calculations.

The difference in alignment of lamellae in single elbow patterns (E_5, Figure 3a) and paired parallel elbow patterns (E_1 and E_2, Figure 3b) is very similar to that in hybrid system. A bending-unbending transition of PS-*b*-PMMA lamellae is observed for $130° \leq \theta \leq 150°$, and more defects are observed at the bending point of the elbow patterns than in the hybrid material.

Self-Consistent-Field Calculations. In this section we present our 2D self-consistent-field (SCF) results for symmetric PS-*b*-PMMA diblock copolymers. The 2D SCF calculations are performed in the rectangular unit cell shown in Figure 5, where periodic boundary conditions are applied in the x (horizontal) direction and reflecting boundary conditions are applied in the y (vertical) direction. Two parallel walls are placed at a separation distance $D_1 = 100$ nm to represent the topographic elbow patterns. The length of each wall, $L = 312$ nm in this case, together with θ determines the cell size L_y. The cell size L_x is chosen such that, under the periodical

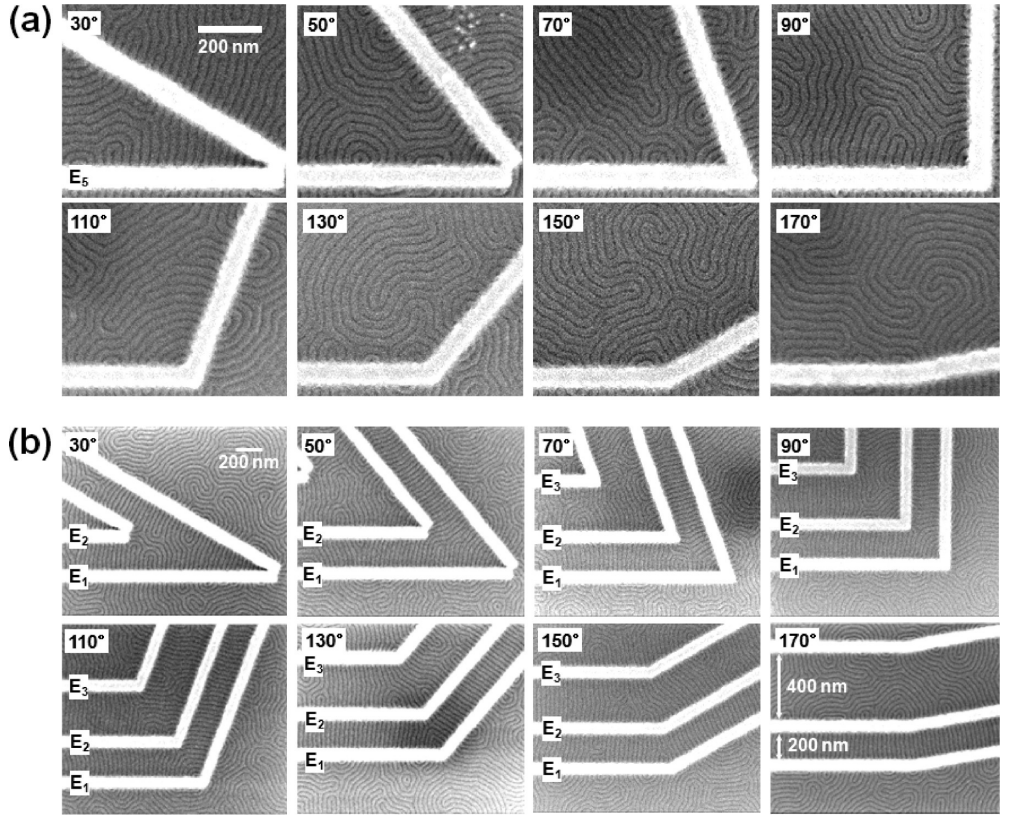

Figure 3. Top-down SEM images of lamellae-forming PS-*b*-PMMA thin films on (a) single and (b) paired elbow patterns with varying angles (θ) from 30° to 170° in 20° increments.

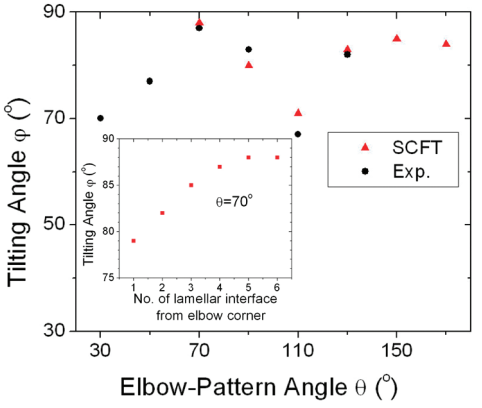

Figure 4. Variation of lamellae tilting angle φ with the elbow pattern angle θ. The inset shows SCF results of φ measured at different lamellar interfaces with $\theta = 70°$.

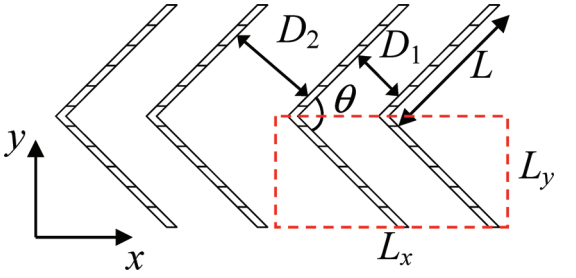

Figure 5. Unit cell (area enclosed by the dashed lines) used in our SCF calculations. The sidewalls of the topographic elbow patterns are represented by the two parallel shaded walls in our unit cell, and the unit cell is duplicated in both x- and y-directions according to the boundary conditions applied.

boundary conditions, the distance D_2 between the two walls as marked in the figure is 200 nm. To exclude copolymers from the regions occupied by the walls while maintaining good numerical performance of SCF calculations,[22] we impose the following overall copolymer segmental density profile in our calculations:[23]

$$\phi_A(\mathbf{r})+\phi_B(\mathbf{r}) = 1+\frac{1}{2}\left\{\begin{array}{l}\tanh\dfrac{[x-x_1(y)]\sin(\theta/2)+\eta}{\tau/4}\tanh\dfrac{[-x+x_1(y)]\sin(\theta/2)+\eta}{\tau/4}\\ +\tanh\dfrac{[x-x_2(y)]\sin(\theta/2)+\eta}{\tau/4}\tanh\dfrac{[-x+x_2(y)]\sin(\theta/2)+\eta}{\tau/4}\end{array}\right\}$$

where $\phi_A(\mathbf{r})$ and $\phi_B(\mathbf{r})$ are the normalized segmental densities (volume fractions) of A and B segments, respectively, at position $\mathbf{r} = (x,y)$; $x_1(y)$ and $x_2(y)$ denote the x-coordinates of the two wall centers, with the relation $|x_2(y) - x_1(y)| = D_1/\sin(\theta/2)$; and we set $\eta = 3.65$ nm and $\tau = 2.92$ nm.

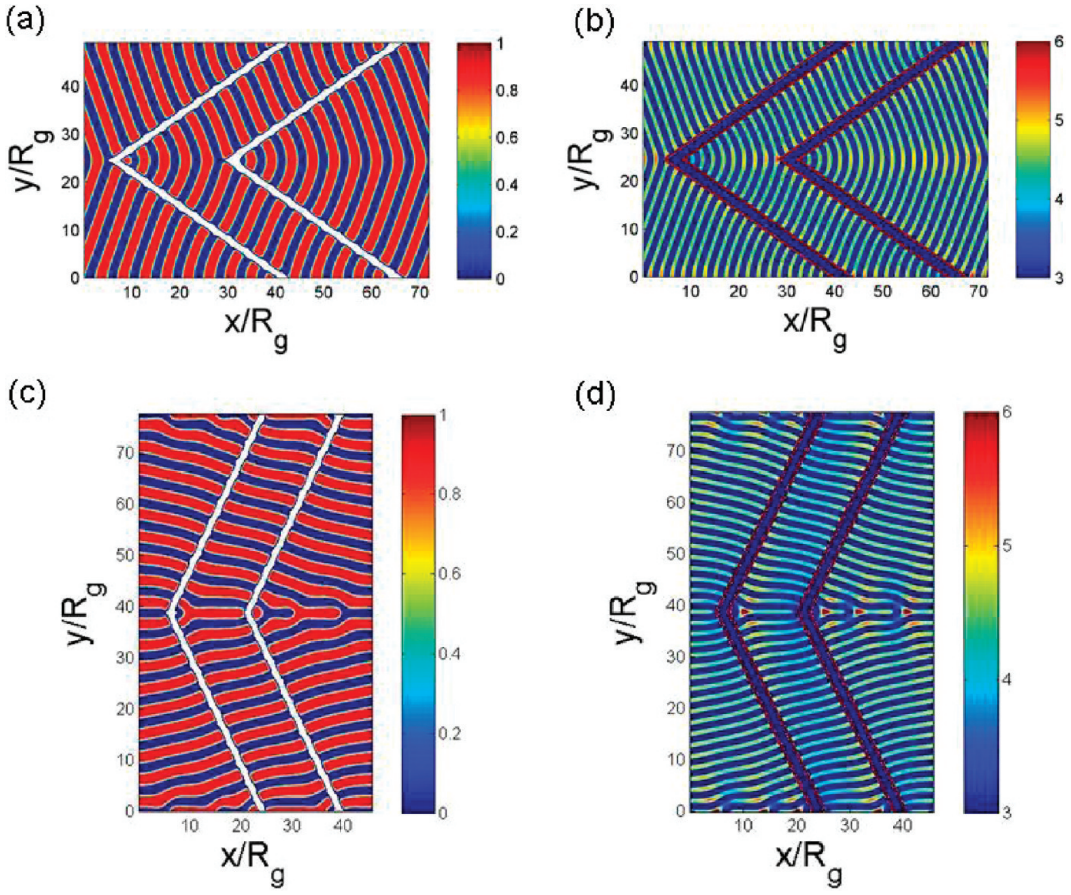

Figure 6. Segmental density profile $\phi_A(\mathbf{r})/[\phi_A(\mathbf{r}) + \phi_B(\mathbf{r})]$ of symmetric diblock copolymers confined between paired elbow patterns at (a) $\theta = 70°$ and (c) $\theta = 130°$, obtained from SCF calculations. The sidewalls are represented by the blank regions in (a) and (c). Parts (b) and (d) show the corresponding distribution of the chain elastic free energy $f_{el}(\mathbf{r})$ in units of k_BT per chain. In all cases, our unit cell is duplicated in the y direction according to the reflecting boundary condition.

In addition to predicting $\phi_A(\mathbf{r})$ and $\phi_B(\mathbf{r})$, that is, the morphology at equilibrium, the SCF calculations further provide us with the corresponding free energy density $f_c(\mathbf{r})$ and its components, which can help identify the formation mechanism of the equilibrium morphology. In particular, the mean-field free energy (of mixing) per chain is $F_c = \int d\mathbf{r}\, f_c(\mathbf{r})/\bar{\phi}_C V$, where V is the system volume and $\bar{\phi}_C = \int d\mathbf{r}\, [\phi_A(\mathbf{r}) + \phi_B(\mathbf{r})]/V$ is the average copolymer segmental density, and $f_c(\mathbf{r})$ has two contributions: $f_{AB}(\mathbf{r}) \equiv \chi N \phi_A(\mathbf{r})\phi_B(\mathbf{r})$ corresponds to the local repulsion between A and B segments, and the chain elastic free energy density $f_{el}(\mathbf{r})$ is associated with the chain conformational entropy.

Figure 6a,c shows the segmental density (volume fraction) profiles of lamellae confined in paired elbow patterns at different elbow pattern angles θ obtained from SCF calculations. When $\theta = 70°$ (Figure 6a), the lamellar domains form arc structures in the inner regions close to the elbow corners and bend structures farther away from the corners. Such structures were referred to as "chevron" kinks by Gido and Thomas.[24] The bend structures terminate in the linear regions of the elbow patterns, where aligned lamellae connecting the sidewalls form. Similar results are also found at $\theta = 90°$ and 110° (data not shown). At $\theta = 130°$ (Figure 6c) and 150° (data not shown), the SCF calculations show that the lamellae break and form "Omega" kinks[24] in the inner regions close to the elbow corners. Finally at $\theta = 170°$ (data not shown), only aligned lamellae connecting the sidewalls are obtained. These morphologies are in good agreement with the experimental observations discussed above when $\theta \geq 50°$. Note that the experimental results exhibit more defects, partly due to the larger gap width than that used in our calculations; on the other hand, we have used different initial guesses in our SCF calculations and at each θ only the morphology with the lowest F_c (i.e., the equilibrium morphology) is presented.

The tilting angle φ of lamellar domains with respect to the sidewalls are also measured in SCF calculations. Since the titling angle depends on the distance from the elbow corner, we measure φ at the fifth lamellar interface from the elbow corner in the larger gap, in accordance with the experiments. The tilting angle is 90° when lamellae are confined between two parallel neutral walls. For lamellae confined between paired elbow patterns, the SCF results in Figure 4 show that φ first decreases with increasing θ and then increases abruptly to ~90° at $\theta = 130°$. These are in good agreement with the experimental data also shown in Figure 4.

The variation of φ with θ can be understood from the free energy densities provided by the SCF calculations. Figure 6b shows the chain elastic free energy density $f_{el}(\mathbf{r})$ at $\theta = 70°$, where $f_{el}(\mathbf{r})$ is high in the middle of A-rich and B-rich domains (due to the localization of chain ends) and even higher at the bend vertices. These peaks indicate that the formation of bend structures involves significant penalty in chain conformational entropy. To reduce the degree of bending of lamellae and thus alleviate such a high entropic penalty, lamellae tilt at an angle $\varphi < 90°$ with respect to the sidewalls. Since a neutral sidewall promotes perpendicular lamellae orientation,[22] a tilting angle $\varphi < 90°$ increases the chain elastic free energy close to the wall. In other words, there is a balance between the bending and tilting of lamellae

confined between the elbow patterns. As θ increases from 70° to 110°, reducing the lamellae bending at the cost of increasing lamellae tilting dominates, which explains the decrease in φ.

As θ further increases, decreases in φ are not sufficient to reduce the bending penalty. Lamellae thus break and form "Omega" kinks, i.e., defects with highly localized chain elastic free energy density as shown in Figure 6d. This behavior is more effective in reducing the entropic penalty in other regions and thus lowering the overall free energy of the system. Therefore, φ increases abruptly to almost 90° when $\theta = 130°$.

Because of the large cell size (L_x) required for smaller elbow corner angles, SCF calculations were not performed for $\theta < 70°$. The bending of lamellae in such cases, however, can be inferred from the results at $\theta = 70°$, where, as lamellae move closer to the elbow corners, the space in between the elbow patterns becomes smaller. In such small confined spaces, forming bend structures with vertices of high elastic free energy density is not favored; instead, arc structures with less bending (no vertices) form. The same phenomenon occurs as θ decreases, where lamellae tend to form arc structures as shown in Figure 3b at $\theta = 30°$. The lamellae bending is therefore reduced at the cost of increasing lamellae tilting. This is clearly shown by the results in the inset of Figure 4 at $\theta = 70°$, where φ decreases as lamellae move closer to the elbow corner, in accordance with the decrease of φ as θ decreases from 70° to 30° as observed in experiments.

Finally, it should be noted that, using 2D SCF calculations in reciprocal space, Matsen[25] and Duque et al.[26] studied kink boundaries between two lamellar grains in bulk. For symmetric diblock copolymers at $\chi N = 20$, Matsen found "chevron" kinks when the angle θ_0 between the lamellar normals of the two grains was less than 78° and "Omega" kinks when $\theta_0 > 104°$.[25] In this study, the lamellar interfaces near the sidewalls were not always straight as shown in Figure 6. If we approximate $\theta_0 \approx \theta + 2\varphi - 180°$, however, our real-space SCF results are consistent with those of Matsen. It is interesting to note that both A and B domains in our "Omega" kinks form elongated protrusions, as shown in Figure 6b, similar to Figure 7d in ref 26. An important difference between the bulk systems studied in refs 24-26 and our confined systems is that the defects are nonequilibrium structures in the bulk but are equilibrium structures in the confined systems.

Conclusion

This work demonstrates that bending and arc geometries of lamellar microdomains in block copolymer films can be formed within angled corners of topographic guiding patterns that exhibit a nonselective wetting property, thereby providing an important extension of the capabilities of the graphoepitaxial technique which is currently limited to creating straight line/space patterns either parallel or perpendicular to the sidewalls of guiding patterns. We used lamellae-forming PS-*b*-PEO/OS hybrid and organic PS-*b*-PMMA diblock copolymers that revealed similar bending trends. For the single elbow pattern, lamellar domains formed closed loop geometry between two linear sections of an elbow when $\theta \leq 110°$, and bending-unbending transition of lamellae occurred at $110° \leq \theta \leq 130°$. For paired elbow patterns, bending and arc geometries of lamellar microdomains were formed when $\theta \leq 130°$, induced by a delicate balance between the lamellae bending and tilting with respect to the sidewalls, while for $\theta \geq 130°$ lamellae broke and "Omega" kinks were formed. The formation of these structures is well explained by 2D real-space self-consistent-field calculations, which provide additional free energy information and are in good agreement with experiments. The ability to generate nonlinear geometries of lamellar microdomains using neutral topographic guiding patterns where the degree of angled topographic patterns governs the bending of lamellae assembly is of significant importance, since it could open new design rules for surface patterning for a wide range of applications including semiconductor device fabrications.

Acknowledgment. Q.W. and D.S.D. gratefully acknowledge the funding from U.S. Department of Energy (DE-FG02-07ER46448) for the self-consistent-field calculations reported in this work. We thank M. Hart and A. Friz at IBM Almeden Research Center for their help in plasma etching. S.-M. Park thanks JSR Micro Co. for their support.

References and Notes

(1) Hawker, C. J.; Russell, T. P. *MRS Bull.* **2005**, *30*, 952.
(2) Segalman, R. A. *Mater. Sci. Eng., R* **2005**, *48*, 191.
(3) Stoykovich, M. P.; Nealey, P. F. *Mater. Today* **2006**, *9*, 20.
(4) Kim, H.-C.; Hinsberg, W. D. *J. Vac. Sci. Technol. A* **2008**, *26*, 1369.
(5) Mansky, P.; Russell, T. P.; Hawker, C. J.; Mays, J.; Cook, D. C.; Satija, S. K. *Phys. Rev. Lett.* **1997**, *79*, 237.
(6) Mansky, P.; Liu, Y.; Huang, E.; Russell, T. P.; Hawker, C. J. *Science* **1997**, *275*, 1458.
(7) Kim, S. O.; Solak, H. H.; Stoykovich, M. P.; Ferrier, N. J.; de Pablo, J. J.; Nealey, P. F. *Nature* **2003**, *424*, 411.
(8) Cheng, J. Y.; Rettner, C. T.; Sanders, D. P.; Kim, H.-C.; Hinsberg, W. D. *Adv. Mater.* **2008**, *20*, 3155.
(9) Park, S.-M.; Berry, B. C.; Dobisz, E.; Kim, H.-C. *Soft Matter* **2009**, *5*, 957.
(10) Park, S.-M.; Park, O. H.; Cheng, J. Y.; Rettner, C. T.; Kim, H.-C. *Nanotechnology* **2008**, *19*, 455304–1.
(11) Park, S. -M.; Stoykovich, M. P.; Ruiz, R.; Zhang, Y.; Black, C. T.; Nealey, P. E. *Adv. Mater.* **2007**, *19*, 607.
(12) Rockford, L.; Liu, Y.; Mansky, P.; Russell, T. P.; Yoon, M.; Mochrie, S. G. J. *Phys. Rev. Lett.* **1999**, *82*, 2602.
(13) Stoykovich, M. P.; Muller, M.; Kim, S. O.; Solak, H. H.; Edwards, E. W.; de Pablo, J. J.; Nealey, P. F. *Science* **2005**, *308*, 1442.
(14) Wilmes, G. M.; Durkee, D. A.; Balsara, N. P.; Liddle, J. A. *Macromolecules* **2006**, *39*, 2435.
(15) Cheng, J. Y.; Pitera, J.; Park, O. H.; Flickner, M.; Ruiz, R.; Black, C. T.; Kim, H.-C. *Appl. Phys. Lett.* **2007**, *91*, 143106.
(16) Jeong, S.-J.; Kim, J. E.; Moon, H.-S.; Kim, B. H.; Kim, S. M.; Kim, J. B.; Kim, S. O. *Nano Lett.* **2009**, *9*, 2300.
(17) Shin, D. O.; Kim, B. H.; Kang, J.-H.; Jeong, S.-J.; Park, S. H.; Lee, Y.-H.; Kim, S. O. *Macromolecules* **2009**, *42*, 1189.
(18) Park, S.-M.; Rettner, C. T.; Pitera, J. W.; Kim, H.-C. *Macromolecules* **2009**, *42*, 5895.
(19) Freer, E. M.; Krupp, L. E.; Hinsberg, W. D.; Rice, P. M.; Hedrick, J. L.; Cha, J. N.; Miller, R. D.; Kim, H.-C. *Nano Lett.* **2005**, *5*, 2014.
(20) Sundstrom, L.; Krupp, L.; Delenia, E.; Rettner, C.; Sanchez, M.; Hart, M. W.; Kim, H.-C.; Zhang, Y. *Appl. Phys. Lett.* **2006**, *88*, 243107.
(21) Fredrickson, G. H. *The Equilibrium Theory of Inhomogeneous Polymers*; Oxford University Press: New York, 2006.
(22) Meng, D.; Wang, Q. *J. Chem. Phys.* **2007**, *126*, 234902.
(23) Khanna, V.; Cochran, E. W.; Hexemer, A.; Stein, G. E.; Fredrickson, G. H.; Kramer, E. J.; Li, X.; Wang, J.; Hahn, S. F. *Macromolecules* **2006**, *39*, 9346.
(24) Gido, S. P.; Thomas, E. L. *Macromolecules* **1994**, *27*, 6137.
(25) Matsen, M. W. *J. Chem. Phys.* **1997**, *107*, 8110.
(26) Duque, D.; Katsov, K.; Schick, M. *J. Chem. Phys.* **2002**, *117*, 10315.